ADVANCED ENGINEERING MATERIALS
www.aem-journal.com

Tailoring the Dynamic Actuation of 3D-Printed Mechanical Metamaterials through Inherent and Extrinsic Instabilities

Zacharias Vangelatos, Zhizhou Zhang,* Grace X. Gu,* and Costas P. Grigoropoulos**

The design of smart flexible structures, such as controlled waveguides or soft robotics, has been accentuated, because they can accomplish energy harvesting, precise motion, and high rigidity. Advanced 3D printing techniques are used to improve these designs through the fabrication of complex 3D architected structures encompassing nonlinear elastic behavior. Nevertheless, the materials used for the fabrication process are also highly viscoelastic, obstructing high deformations or the transport of mechanical signals due to high energy dissipation. Herein, how the resonance of 3D-printed structures that require large actuations can be tailored through inherent and extrinsic instabilities is demonstrated. The 3D complex structures are designed such that buckling is evinced, ushering large deformations. In addition, prebuckling of the undeformed samples substantially diminishes the effective viscosity of the structure. Performing vibrational response simulations on both the undeformed and the prebuckled designs and high-speed imaging on fabricated samples, it is observed that the resonant frequency amplitude is enhanced, more resonant frequencies are reinvigorated, and deformation transcends through the whole structure. The results promulgate the utility of the architected design, combined with controlled instabilities, in the modeling of complex smart structures facilitating large deformations, low energy dissipation, and controlled stiffness.

1. Introduction

Architected materials have facilitated a significant breakthrough in the control of the mechanical behavior of structures. Most notably, metamaterials with unprecedented properties can be easily designed in large scales, exhibiting high strength,[1] tunability of their properties,[2] resilience or versatility to large deformations,[3,4] and auxetic behavior.[5] In addition, 4D printed structures can modify their shape depending on the working environment.[6] Due to their chemical composition, these structures can modify their mechanical and electrochemical properties based on external stimuli.[7] This mechanism has substantial implications on the mechanical response of the material, furnishing stiffening of the structure or malleability on demand. Furthermore, designing structures that are also adaptive to actuation has given rise to the design of flexible 3D-printed mechanisms.[8] Flexible structures can be utilized for engineering applications requiring large but recoverable deformations, continuous motion, and high precision. A characteristic category of structures encompassing these properties are soft robotics. Soft robotic mechanisms are composed of rubber materials that can be electrically actuated to sustain nonlinear deformations.[9,10] Combining these designs with much stronger fiber components leads to the design of artificial muscles,[11] imitating animal motion[12] and having a significantly higher strength than simple soft robot systems.[13–15] Nevertheless, metamaterials also exhibit remarkable properties that are not observed in conventional systems. A characteristic example is the transport of mechanical signals with the proclivity to a specific direction. This has been accomplished through the design of nonreciprocal mechanical metamaterials.[16] In regular materials, the transmission of any physical quantity, such as mechanical signals or mechanical waves, is identical, regardless of geometrical or material asymmetries and defects between any two points in space. However, nonreciprocal metamaterials can alter this behavior, giving directionality to the transport of these mechanical quantities. This is the paragon of the next-generation mechanical signal transport,[17] isolation,[18] and energy storage.[19] In addition, the combination of the architected design with the macroscopic dynamic loading conditions can provide the formation of distinct elastic vector solitons.[20] These coupled waves can have significantly different formations depending on the direction of the wave, controlling not only the direction of the signal, but also its shape. The inexorable advances in 3D printing technology have enabled the fabrication of these structures. Techniques such as fused deposition modeling (FDM),[21]

Z. Vangelatos, Z. Zhang, Prof. G. X. Gu, Prof. C. P. Grigoropoulos
Department of Mechanical Engineering
University of California, Berkeley
Berkeley, CA 94720, USA
E-mail: zacharias_vangelatos@berkeley.edu; zz_zhang@berkeley.edu; ggu@berkeley.edu; cgrigoro@berkeley.edu

Z. Vangelatos, Prof. C. P. Grigoropoulos
Department of Mechanical Engineering
Laser Thermal Laboratory
University of California, Berkeley
Berkeley, CA 94720, USA

Z. Zhang, Prof. G. X. Gu
Gu Research Group
Department of Mechanical Engineering
University of California, Berkeley
Berkeley, CA 94720, USA

The ORCID identification number(s) for the author(s) of this article can be found under https://doi.org/10.1002/adem.201901586.

DOI: 10.1002/adem.201901586

polyjet,[22] selective laser sintering (SLS),[23] and stereolithography (SLA)[24] can realize the inherent challenge to create these structures with high resolution. Even though there has been tremendous progress to expediate these fields, there are still elusive design challenges originating from the used materials. Most notably, rubber materials used in these additive manufacturing techniques exhibit high viscoelastic effects. The repercussions are high energy dissipation, hampering the mechanical deformation propagation along the structure. To accommodate this, high-power actuation systems must be used to outbalance the mechanical losses, increasing the cost and complexity of the design for dynamic control,[14] or conduct benchmark tests on small-scale structures. Another method is to tailor the geometry of the structure to create multiple equilibrium positions that the material can store and release energy. This mechanism is based on bistability and controlled snap through buckling on the structure.[25] Buckling is a state of instability in the material leading to large deformations. Nevertheless, it can be an imperative mechanism to design metamaterial structures, as it determines the effective properties of the medium, such as auxetic behavior[26] or high energy absorption.[19] For hyperelastic materials, this deformation is reversible and therefore efficient for soft robotic applications and 4D printed materials that function in this deformation regime.[6] Nevertheless, buckling is not sufficient to mitigate the effective viscosity of the material.[27] Bistability can provide deformation propagation, effectively vanishing the viscoelastic effects.[28] The physical principle is associated with the local maxima and minima of the potential energy. Even though this mechanical principle is highly efficient to supersede the limitations of the viscoelastic material, it has been studied for 2D structures,[29] whereas the design of 3D structures is still tenuous. Furthermore, even though all of these effects have been studied under the scope of wave mechanics, their dynamic and vibrational response that has been reported is incipient, especially for 3D structures. The dynamic response of the system is imperative to determine its efficient control scheme, such as proportional integral derivative (PID) control, and characteristic behavior.[30] In this study, we demonstrate an alternative approach to this design challenge. We design novel 3D metamaterial structures possessing large deformations, hyperelastic behavior, and mitigated viscosity at vibrations of different frequencies. These structures incur innate and extrinsic instabilities that cause buckling. These effects combined can enhance the malleability and enable the actuation propagation through the whole structure, circumventing the dependence on multiple equilibrium positions. It is also observed that there are significant changes in the creep compliance of the structure and subsequently, to its relaxation modulus. The consequence is a substantial effect on the dissipation losses and the stiffness of the material. To instantiate this principle, a 3D metamaterial unit cell is architected such that buckling commences at the early stages of deformation, facilitating large deflections. The mechanical response is examined using nonlinear finite element analysis (FEA). In addition, by prebuckling the undeformed structures, we elicit how the viscoelastic effects diminish, leading to the actuation of the whole assembly. Prebuckling makes the whole system highly nonlinear, and it greatly enhances the deformation in the resonant frequency.[31] By studying the dynamic response of the structure through experiments and simulations, we reveal intriguing effects regarding the augmented amplitude of the structure at the resonant frequency and activation of more resonant frequencies. In addition, it is investigated how these effects are evinced for different spatial configurations of unit cells. Our findings establish how controlled instabilities bequeathed by design and boundary conditions can surmount the limitations that materials used in 3D printing bear. In addition, soft robotic systems are primarily designed from the perspective of the innate properties of the material, e.g., electrical or chemical actuation. Therefore, from the scope of structural design, 2D structures[14,19] have been thoroughly utilized, because their analysis is easier, whereas the analysis of perplexed 3D designs has been fairly limited.[2,4,8,9] Therefore, we aim to present how 3D printing can be utilized to its full potential, designing complex 3D structures with tailored dynamic properties. Furthermore, 3D design can be used for the control of mechanical signals in multiple directions and for the design of flexible systems with anisotropic 3D mechanical properties, depending on loading conditions and the desired direction of the output.[20] The modeling of the dynamic behavior will also pave the way to efficiently design control systems that will be utilized for the closed-loop control of soft robotic systems. This will mitigate the error to move the system to the desired position or apply the correct amount of force, which demands an in-depth analysis of the dynamic properties of the controlled system.

2. Design of Architected Structures

The candidate-designed unit cells are shown in **Figure 1**A. As the objective is to create a 3D structure, the unit cells are designed such that they have hexagonal symmetry, enabling the 3D spatial configuration of the beam members and the 3D assembly of neighboring unit cells. The beam members are connected on two hexagonal bases at the top and bottom of the unit cell. In addition, the hexagonal base provides easy connectivity with all the unit cells aligned in one orientation. Because each unit cell can be connected with six neighboring ones, the structure can be resilient to out-of-plane buckling. However, as it will be shown later, this is also affected by the number of beam members in the structure. There are two main categories of beam members in the unit cells. The first are the ones connecting the upper and lower base and lies on the faces of the unit cell. The second ones connect the center of each base with the vertices of the other. The number of members of the second category diversifies the two unit cells. For the first unit cell (UC1), only one base is connected to the vertices of the other, rendering it nonsymmetric in the lateral direction, whereas both bases are connected to the vertices of the other in the second unit cell (UC2). This asymmetry in the loading direction is critical for out-of-plane buckling to commence, as demonstrated in Section 3. To facilitate large deformations for actuation, buckling must commence at early stages of the deformation. 3D structures can have multiple different buckling responses, varying from sliding of the unit cells with respect to the others (out of plane buckling), to internal buckling and propagation of the deformation through subsequent layers.[32] Although cubic structures can be considered 3D, they are symmetric with respect to a specific plane, rendering their analysis 2D. These structures have very specific buckling modes

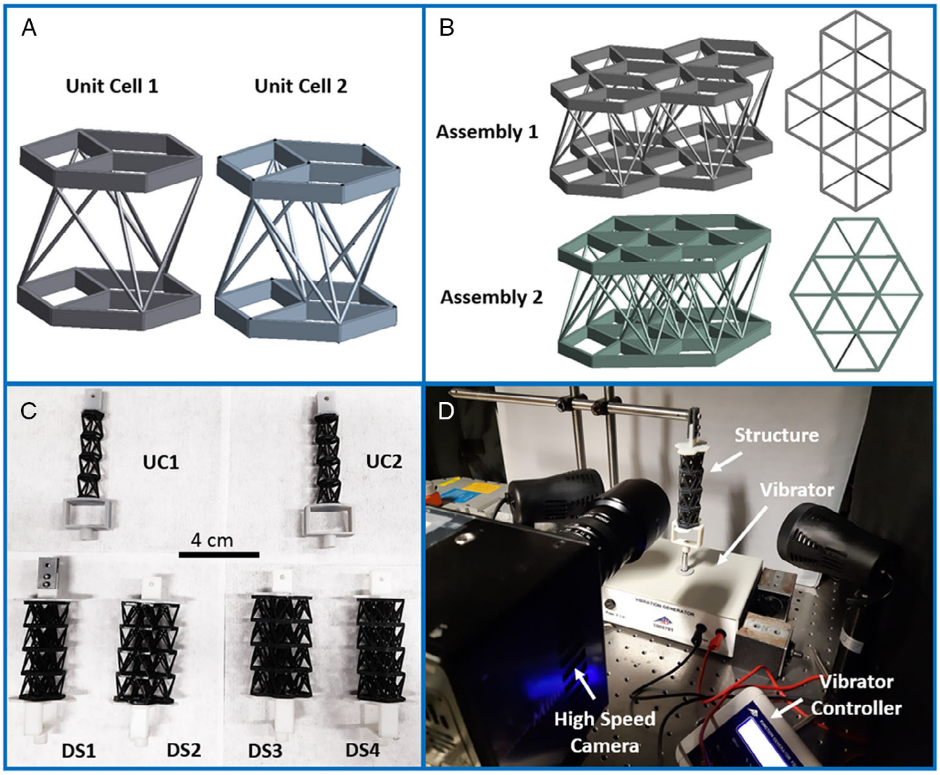

Figure 1. Design and fabrication of the architected structures. A) The two basic unit cells, having nonsymmetry in the lateral direction (unit cell 1) or being symmetric in the lateral direction as well (unit cell 2). B) Potential assemblies of the unit cells, if there is no intersection of the neighboring unit cells (Assembly 1) or the proximal unit cells are intertwined (Assembly 2). C) Characteristic 3D-printed samples for each design and each assembly. D) Side view of the experimental apparatus used for the characterization of the dynamic response as a function of the frequency. A high-speed camera is focused on specific layers of the structure, enabling the high spatial and temporal resolution of the deformation.

that depend on the macroscopic loading conditions.[33] For 3D structures, the buckling modes are associated with the dimensions of the geometry, providing multiple design choices for the same structures depending on the design constraints. In our previous work, we instantiated these principles utilizing unit cells designed with curved beams instead of straight.[32] This effect can lead to postcontact and it will stiffen the unit cell. Postcontact is imperative to make the stiffness of the structure positive after buckling commences, which leads to negative stiffness. This design paradigm will imitate a snap-through mechanism that can lead to a local equilibrium of the potential energy in static loading. Nevertheless, this design will be egregious for our current objective, as it will prohibit larger deformations due to densification of the unit cell. Establishing large deformations as the inherent characteristic of the structure is the main goal of this study. Therefore, stiffening due to postcontact is diminished using straight beam members instead of curved ones. As shown later, the effect of stiffening can be manifested in viscoelastic materials through frequency control, which is based on material property instead of a designing tactic.[27] Furthermore, functional architected materials have to be used in periodic 3D arrays in the structure. Because the unit cells are 3D, they can be assembled either by connecting the edges of each base (Assembly 1) or by intertwining them, connecting the central plates of the bases (Assembly 2).[34] Both assemblies are shown Figure 1B. To validate their dynamic behavior, each geometry was fabricated by 3D printing. The material of the base is selected to be stiffer than that of the beams to forestall excessive deformation of the base, because this mechanism will obstruct the buckling of the beams. The reason is that if the base has the same stiffness as the material, they cannot be considered fixed supports but torsional and bending springs. Then, the structure will have the predilection to bending and shear deformation, purloining a portion of the strain energy that accounts to compression. Compression is the only deformation mode that transcends into buckling. Even though bending and buckling have similar macroscopic features, buckling as an instability mechanism can facilitate large deformations for the whole structure.[33] Further details regarding the 3D printing process are provided in SI1, Supporting Information. The periodic arrays that utilize Assembly 1 with unit cell 1 (DS2) and unit cell 2 (DS3) and Assembly 2 with unit cell 1 (DS1) and unit cell 2 (DS4) are shown in Figure 1C. A characteristic configuration of a fabricated sample on the vibration apparatus with respect to the imaging system is shown in Figure 1D. Detailed information regarding the experimental setup is provided in SI2, Supporting Information.

To validate the intrinsic instability that the structures must embrace, nonlinear FEA analysis was used to investigate whether any of the unit cells will reach a cauldron, teetering.

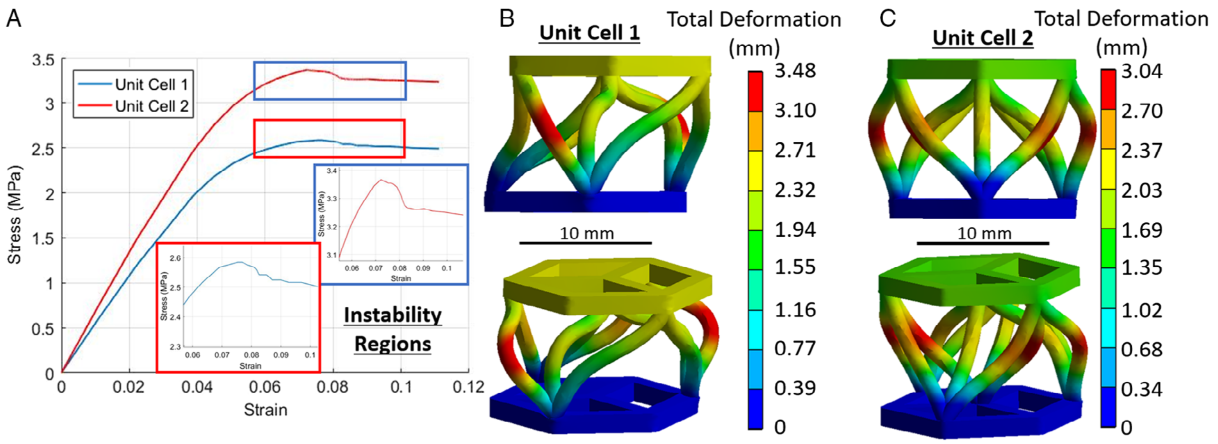

Figure 2. Nonlinear FEA analysis for UC1 and UC2. A) Stress–strain response of the two unit cells. For the unit cell 1, buckling commences at 7.7% lateral compression, whereas for unit cell 2, it occurs at 7.2%. B) The deformation field on unit cell 1. Because this unit cell is not symmetric in the lateral direction, out-of-plane buckling commences, creating a nondesired deformation mode. C) The deformation field on the unit cell 2. The buckling leads to the external opening of the structure, avoiding in-plane buckling and subsequent postcontact that will stiffen the structure and apprehend the deformation propagation.

Details on the modeling and the constitutive equations that must be solved are provided in SI3, Supporting Information. **Figure 2** shows the simulated behavior for both unit cells. Figure 2A shows that both unit cells become unstable during the early stage of the deformation ($\varepsilon_{\text{total}} = 7.7\%$ and 7.2% at $\sigma_{\text{lateral}} = 2.5$ and 3.367 MPa for UC1 and UC2, respectively). UC1 has less members than UC2; therefore, its resilience is lower, leading to instability at a lower load. The reason is that the critical buckling load is proportional to $\approx EI_{\text{eff}}/L_{\text{eff}}$, where E is Young's modulus, I_{eff} is the effective bending inertia of the structure, and L_{eff} is the effective length of the beam based on its boundary conditions. As both structures have the same boundary conditions, they have the same effective length. Nevertheless, the effective inertia depends on the effective cross-section of all the beams. Therefore, less beam members will lead to a decrease in I_{eff}, as validated by the simulation results. After the buckling event, the slope remains negative, because the unit cells are designed such that there is no postcontact of the proximal beams.[32] However, they have two distinct buckling mechanisms, as shown in Figure 2B,C. UC1, as it is asymmetric with respect to the loading direction, is subject to out-of-plane buckling. This leads the top base to "slide" with respect to the other. This mechanism is not observed in UC2, where the symmetry enables the unit cell to expand uniformly in the radial direction. Furthermore, it must be noted that the asymmetric loading will lead to higher stress distribution at some nodes, leading to failure at the resonant frequency for a small number of cycles. Thus, UC1 is inadequate to provide a steady propagation of the deformation that is required for soft robotic applications for instance. As shown later, a periodic assembly can alleviate this effect, but it will still be observed as it is inherited by the unit cell encompassing this behavior. This result will foreshadow that assemblies with UC2 will likely be better design choices. With the mechanical response of the unit cells delineated, the mechanical response of the unit cells during vibration can be interpreted.

3. Results and Discussion

3.1. Dynamic Response of Unblemished and Prebuckled Unit Cell Structures

Utilizing the experimental apparatus shown in Figure 1D, arrays of fabricated individual unit cell structures were tested in vibrations as a function of the frequency. Each array consists of four layers. The unit cells have a height of 18 mm and beam diameter of 1 mm. These dimensions were selected such that the maximum resolution of the 3D printer can be used. Smaller unit cells can be utilized for smaller-scale applications that require small but complex structural features that embrace metamaterial behavior. In addition, a large number of unit cells can be utilized for applications requiring large-scale but stable mechanisms.[29] Tacitly, based on the previous investigation of scale effects,[32] increasing the thickness of the beams will lead to nondesired postcontact at early stages of deformation. Because one of the common repercussions of 3D printing is nonuniform material properties, larger unit cells will also be more susceptible to material inhomogeneity, ushering nonsymmetric deformation due to material properties rather than a rigorous design approach. Although scale effects are not pertinent for this study, future work should also focus on their consequences on 3D printing structures and how material inhomogeneity affects the frequency response. To monitor the experimental results, harmonic response simulations were conducted to attain the Bode plot of the amplitude as a function of the frequency. Further details on vibrational analysis are provided in SI3, Supporting Information.

Representative curves of the normalized amplitude as a function of the frequency for both unit cells are shown in **Figure 3**. For both structures, there is close match between the experiments and the simulations, indicating that the modeling used by the FEA solver can depict the realistic behavior of the structures. The variance may be associated with inhomogeneities in the material that would be significantly more predominant for larger and

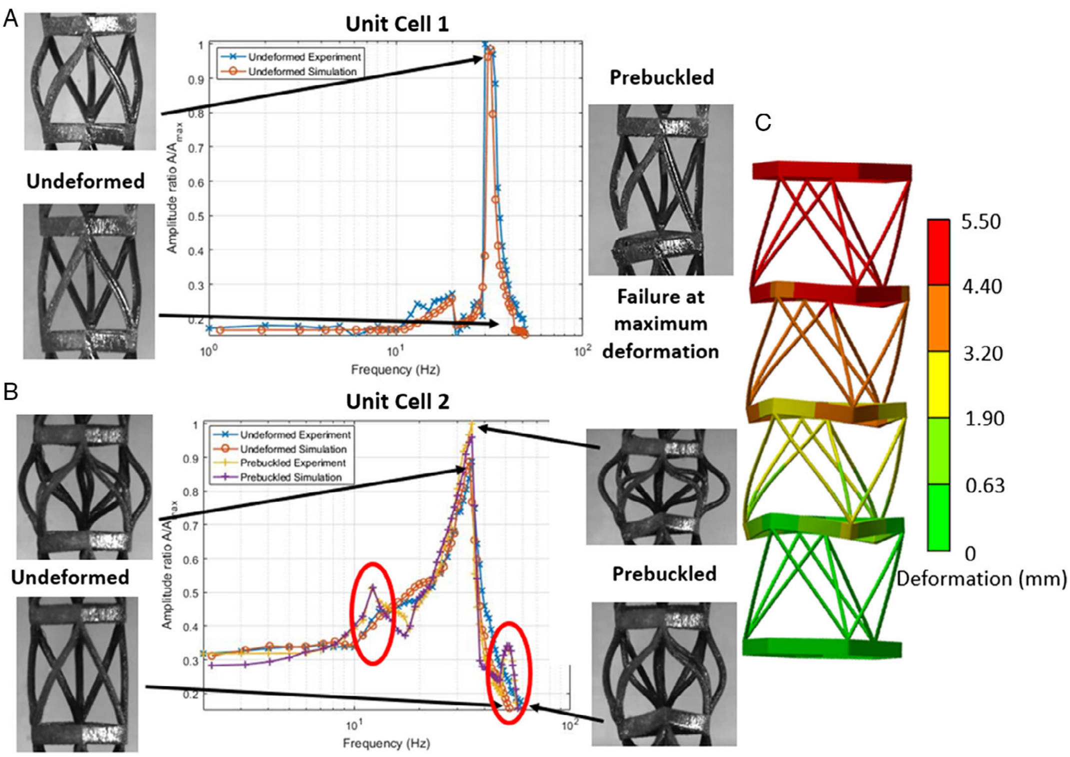

Figure 3. Comparison of the harmonic response and the experimental response for UC1 and UC2. A) Normalized deformation amplitude–frequency curves for UC1. The resonant frequency is at 32 Hz but the small number of beam members renders it susceptible to failure due to the dynamic loading at prestressing. B) Normalized deformation amplitude–frequency curves for UC2. The individual unit cells do not have the structural integrity to have stable vibration propagation through subsequent layers. This out-of-plane instability renders the maximum amplitude the same for both the undeformed and prebuckled configuration. However, apart from the main resonant frequency at 32 Hz, two more are observed at 12.19 and 52.19 Hz (marked in the red circles). C) Characteristic deformation distribution obtained by the harmonic response for the unstressed configuration to obtain the amplitude–frequency curve. The deformed state for both unstressed and prestressed configuration of the tested structures is demonstrated at maximum and minimum deformation.

thicker members and should be investigated in future work. Characteristic deformations obtained for the resonant frequency are shown in Figure 3C, revealing partial bending of the bases and radial expansion of the structure, as in the experiments. The captured deformation at resonant frequency is also presented (Figure 3). Both samples were tested in the initially undeformed and prebuckled configurations (with 2 mm compression). The fact that this state is associated with buckling can be verified by Figure 2A, because at this deformation regime the structure is unstable. In addition, for 2 mm, only buckling at the beams was observed, whereas for higher deformations, overall buckling of the whole structure commences. This causes sliding of the layers, causing out-of-plane buckling for the whole structure. At the resonant frequency, which is equal to 30 Hz for UC1 and 35 Hz for UC2, the amplitude increase compared with low- and high-frequency actuation is 80% and 70%, respectively. Nevertheless, prebuckling renders the individual unit cells highly unstable, as they begin having out-of-plane deformation and not uniform lateral propagation of the deformation into subsequent layers. Therefore, prebuckling does not have a significant effect in the amplitude increase, which becomes significantly large due to out-of-plane deformation. In addition, it must be noted that UC1, having less beam members, exhibits nonsymmetric deformation. Consequently, fracture occurs at some beam members (Figure 3A), as indicated by the nonlinear structural analysis. Moreover, there is a shift of the resonant frequency of the two unit cells. That is a significant change, since the frequency range that dynamic phenomena are observed is only 60 Hz. This implies that the architected design can be used as a tool to switch the resonant frequency of functional materials. Moreover, for the case of UC2, prebuckling leads to the creation of two more resonant frequencies, at 12.19 and 52.19 Hz (by interpolation of the experimental curves). This means that more modal shapes in the structures are activated for lateral loading, a result consonant with the simulations. The harmonic response estimated the values of these resonant frequencies at 12 and 53 Hz, respectively. The variance of the modal shapes and the shifting of the natural frequencies due to prestressing have been reported before,[30,31] and it is consonant with our experimental results. At higher frequencies, the amplitude of the deformation tends to 0, as the inertia of the unit cells cannot follow up the high-frequency actuation, a result consistent with the dynamic behavior of mechanical systems.[35,36]

3.2. Control of the Response of 3D Periodic Assemblies

Furthermore, the four different periodic arrays were tested. The results are presented such that the two different combinations for each assembly are compared. Therefore, the designs

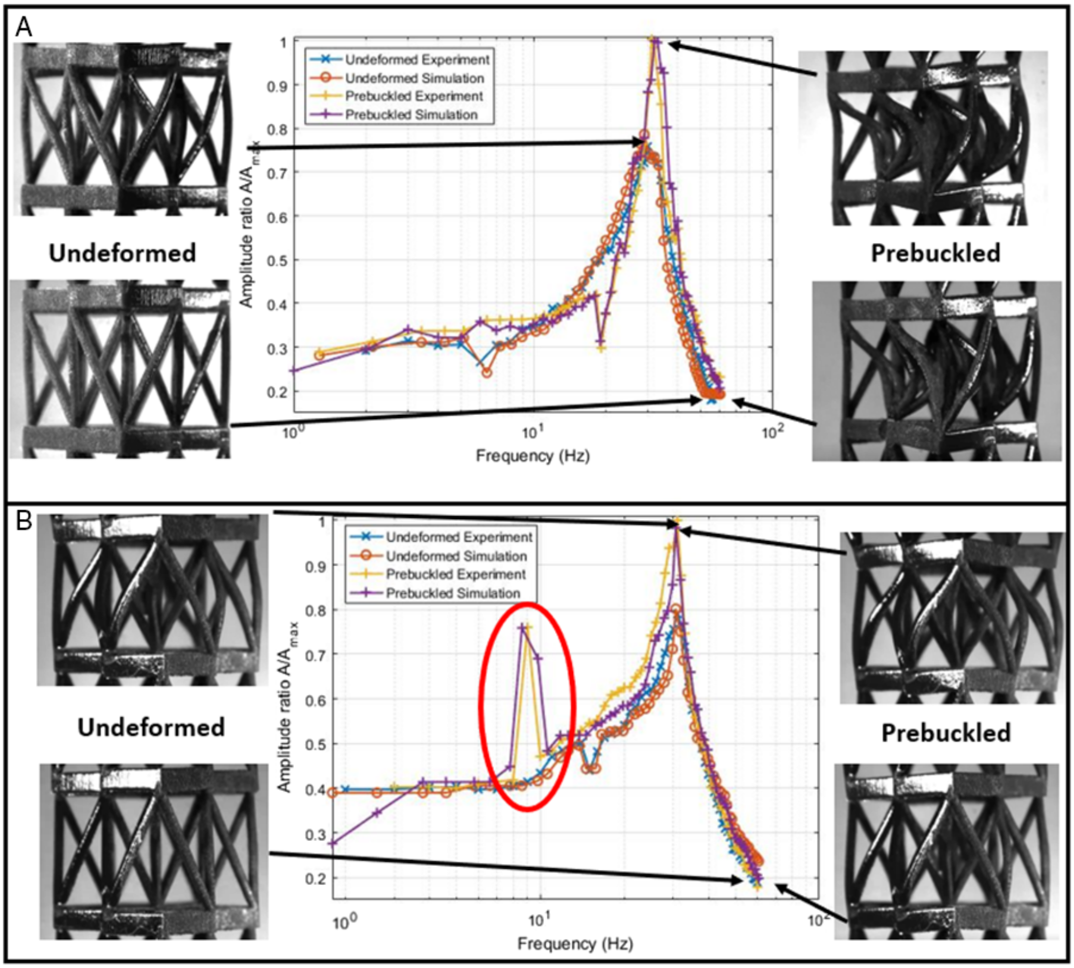

Figure 4. Comparison of the harmonic response and the experimental response for the Assembly 1 with unit cells 1 and 2 (DS1 and DS4). A) Normalized deformation amplitude–frequency curves for DS1. The resonant frequency for the prebuckled structure is at 32 Hz, whereas for the undeformed design it occurs at 29 Hz. B) Normalized deformation amplitude–frequency curves for DS4. Although the main resonant frequency is at 30 Hz for the prebuckled configuration (31 for the undeformed), the amplitude at 9 Hz is also significantly enhanced for the prebuckled configuration (marked in the red circle). The deformed state for both unstressed and prestressed configuration of the tested structures is demonstrated at maximum and minimum deformation.

associated with Assembly 1 (DS1 and DS4) are shown in **Figure 4**, whereas the designs related to Assembly 2 (DS2 and DS3) are shown in **Figure 5**. For DS1, prebuckling precipitates 71% increase in the resonant amplitude compared with low-frequency actuation, whereas an initially undeformed structure has 62% increase. It is observed by the captured frames (Figure 4A) that the out-of-plane deformation commences at the assembly as well, as all the beam members have the proclivity to buckle to the right side of the structure. This is the same mechanism shown for the individual unit cell (Figure 2B). Although this effect is manifested in the initially undeformed assembly as well, it is significantly mitigated as the viscoelasticity causes energy dissipation which is removed by the strain energy caused by buckling. Moreover, there is a shift of the resonant frequency. From 29 Hz for the initially undeformed configuration, it is shifted to 32 Hz due to prebuckling. Recordings of the deformation of the initially undeformed and prebuckled DS1 are provided in V1 and V2, in the Supporting Information, respectively. For DS4, radial expansion is observed (Figure 4B), which is the same deformation mode shown in Figure 2C. Therefore, from a functional standpoint, this design is more efficient as it does not have a detrimental buckling mode.[32] The characteristic responses at the resonant frequencies are provided in V3 and V4, in the Supporting Information. In addition, this assembly has more beam members, leading to a 49% increase in amplitude at the resonant frequency (at 31 Hz). This result is reasonable, considering that more beam members increase the rigidity of the structure. However, prebuckling increases the amplitude to 61%, whereas there is also a small shift of the resonant frequency (at 30 Hz). It must be remarked that there is also a new resonant frequency at 9 Hz, which is comparable with the amplitude of the initially undeformed structure.

Examining the response of the two structures, similar instability mechanisms occur even at the intertwined beam members (Figure 5). In DS2, the layers face out-of-plane deformation for both undeformed and prebuckled configurations (Figure 5A),

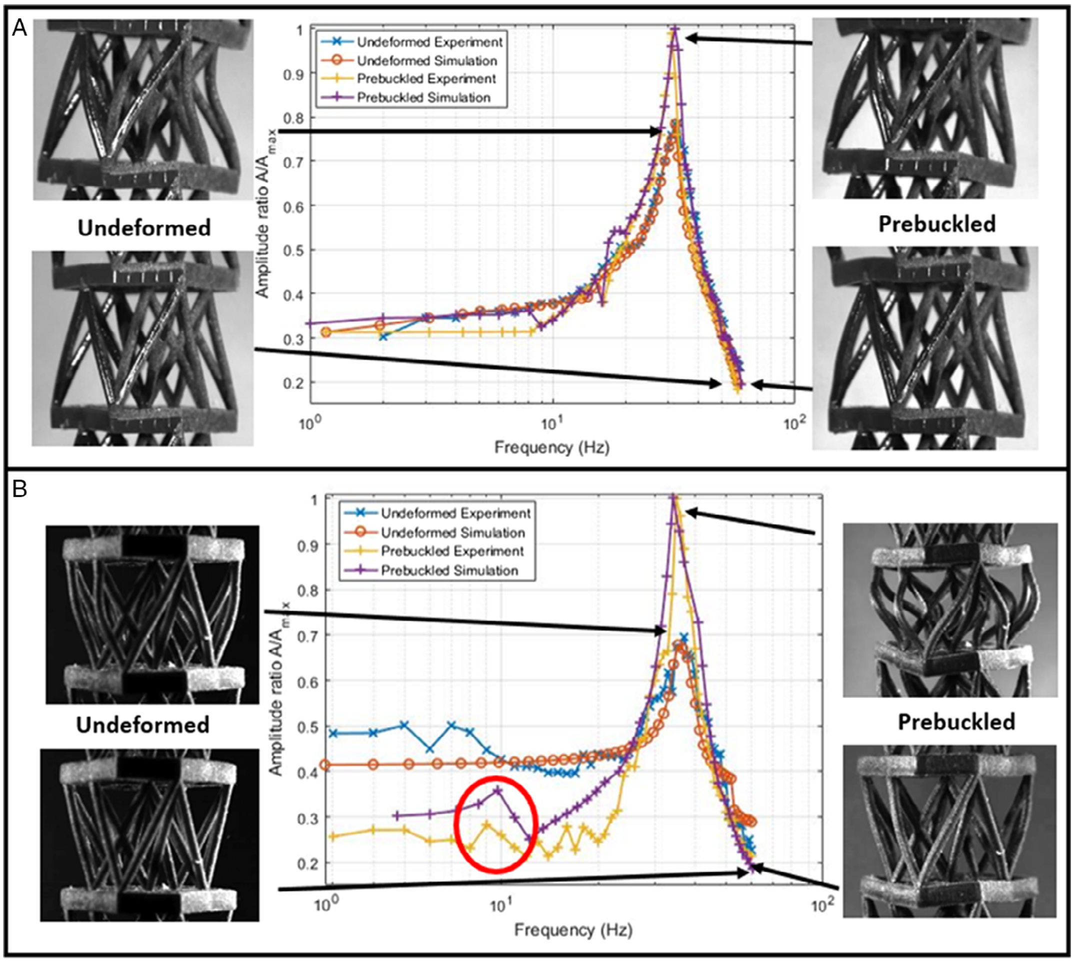

Figure 5. Comparison of the harmonic response and the vibrational response for the Assembly 2 with unit cells 1 and 2 (DS2 and DS3). A) Normalized deformation amplitude–frequency curves for DS2. The resonant frequency is at 32 Hz and there is a significant variation of the amplitudes for the unstressed and prestressed configuration. B) Normalized deformation amplitude–frequency curves for DS3. The main resonant frequency is still at 32 Hz and again there is another resonant frequency at 10 Hz (marked in the red circle). The deformed state for both unstressed and prestressed configurations of the tested structures is demonstrated at maximum and minimum deformation.

and DS3 faces radial expansion due to buckling (Figure 5B). The resonant frequency of DS2 does not show a remarkable change, shifting from 32.16 to 32 Hz. Moreover, the amplitude increase at the resonant frequency increases from 60% to 68%. This result is a repercussion of the design of Assembly 2. The beam members are intertwined in comparison with Assembly 1, leading to significant increase in the rigidity. DS3 proved to be a much more efficient design, as the amplitude from low frequency to resonant frequency increased from 35% to 77%, at 37 and 35 Hz, respectively.

Regardless of the amplitude increase, it is imperative to create a design that can vanish the viscoelastic effects and promote uniform deformation propagation through the whole structures. To capture this, the deformation at the layer which is the farthest from the vibrator was observed for all the samples. The reason why the Bode plots of the amplitude were measured at the initial layers was that there is minuscule deformation of the undeformed structures at the top layers. Therefore, the variance of the amplitude as a function of the frequency could be distinguished using image processing on the captured deformations. Representative recordings for DS3 and DS1 are given in V5, V6 and V7, V8, in the Supporting Information, respectively. As indicated by the measured deformation shown in **Figure 6**, all the designs show a remarkably larger deformation at the final layer in the prebuckled state. This leads to five times amplitude increase at the final layer (DS1). DS2 has a 2.22 times larger deformation, whereas DS3 and DS4 have a 3.5 and 3.36 times larger deformation, respectively. To fathom this effect, the amplitude increase must be correlated with the energy dissipation of the viscoelastic material. Because for all of the experiments either one or two peaks were observed, the system behaves like a second-order system or two convoluted second-order systems (i.e., fourth order). These systems can be characterized by their natural frequency ω_n and their damping coefficient ζ. Using the analysis presented in SI4, Supporting Information, the damping capacity of the material, which is the ratio of the energy dissipated over the energy stored, is proportional to $\sum_{i=1}^{2} \frac{2\zeta_i \omega_{ni} \omega}{(\omega_n^{i2} - \omega^2)}$,

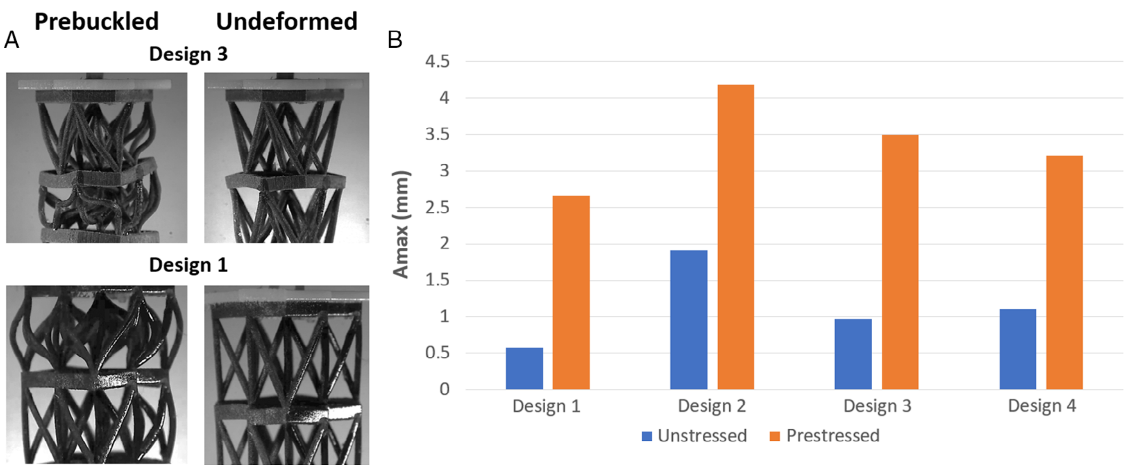

Figure 6. The deformation amplitude for each structure at the last layer in the prestressed and unstressed configuration. A) Characteristic response at the final layer for the prestressed and unstressed configuration. It is observed that the prebuckled configuration has significantly a larger deformation on the final laye,r providing the actuation propagation through the whole structure. B) Deformation comparison for both configurations at the last layer, accomplishing an increase in the amplitude at 500% for DS1 or 222% for DS2, 350% for DS3,% and 336% for DS4.

where ω is the frequency of the applied force. Because the peaks of the resonant frequencies are proportional to $1/\zeta$, the increase in the amplitude of deformation leads to mitigation of the energy dissipation of the whole structure, a conclusion congruous with the experimental results. To put this analysis into perspective, we present the numerical results for DS4, where the amplitude difference is blatant between brebuckled and undeformed configurations. As the amplitudes are normalized, we use an effective damping coefficient $\overline{\zeta}$. By measuring the peaks of the experimental curves, the undeformed structure has $\overline{\zeta}_1^{\mathrm{un}}(\omega_{n1} = 11\mathrm{Hz}) = 2.5$ and $\overline{\zeta}_2^{\mathrm{un}}(\omega_{n2} = 31\mathrm{Hz}) = 1.25$. However, for the prebuckled structures, $\overline{\zeta}_1^{\mathrm{pr}}(\omega_{n1} = 9\mathrm{Hz}) = 1.25$ and $\overline{\zeta}_2^{\mathrm{pr}}(\omega_{n2} = 30\mathrm{Hz}) = 1$. Therefore, the damping capacity of the material decreases in the prebuckled configuration. The measured normalized values of the damping coefficient for each structure are shown in Table S1, in the Supporting Information. However, as viscoelastic materials have fading memory effects, they can behave nonlinearly. This means that the damping coefficient ζ depends on the loading history of the structure. Nevertheless, by conducting all the experiments multiple times, the same resonant frequencies were observed and the amplitude of the prebuckled structures was always higher than that of the initially undeformed structures. Therefore, even though the results will vary depending on the time the measurements are carried out with respect to previous measurements, they can still provide a quantitative argument why prebuckling precipitates the mitigation of viscoelastic effects. Nonetheless, for this analysis to be valid, it is imperative that the mechanical response leads to a closed-loop hysteresis curve in the force–displacement curve. Otherwise, the system has a chaotic behavior that cannot be addressed by the presented analysis.[37] Using image processing on the recording deformations, the deformation of selected layers can be measured as a function of time and compared with the applied force. Further details on this process are presented in SI5, Supporting Information. Characteristic curves for DS4 at the resonant frequency are shown in Figure S1, Supporting Information. It is evident that in the steady state there is a phase difference between the applied force and deformation because the materials are viscoelastic. Plotting the force as a function of the displacement (Figure S2, Supporting Information) reveals that there is indeed a closed hysteresis loop, and the system does not have a chaotic nonlinear behavior.[37] Therefore, the harmonic response analysis can be used.

Despite this intriguing finding, the mechanical responses that were presented must also be put into perspective. The assemblies with UC2 are much more efficient than UC1 because out of plane buckling is hindered. In addition, this design leads to the activation of more resonant frequencies, modifying the frequencies that can be used to actuate the structure. This effect can be rather expedient for mechanisms that need a step-wise actuation, with a large but steady increase in the deformation. There is also a remark that must be addressed regarding the versatility of these materials coupled with architected structures. At higher frequencies, it is observed that all of the structures have miniscule deformations. However, there is another mechanism that is evident at high frequencies. From the theory of mechanical behavior of polymers[27,38] at high frequencies (above 60 Hz for the fabricated structures), the viscosity of the material tends to become 0 (as noted in SI4, Supporting Information), and the material behaves as a rigid structure. This effect, accompanied by the tailored malleability of the prebuckled structures, can lead to adaptive devices[2,39] that show significant versatility in transitory environments requiring either high strength and rigidity or large deformations and flexibility by frequency modulation.

Nevertheless, it must be noted that based on the recorded deformation of the fabricated structures, coupling of multiple loading modes such as torsion is insinuated. This coupling has significant effects on the modal response of dynamic systems, as it has been delineated.[37] Although the modal analysis that was conducted revealed rotational modal modes as well, these responses should have a drastic effect depending on the applied loading of the structure. Future work should focus on the modeling of such coupling in the dynamic response of 3D viscoelastic materials. Furthermore, experimental techniques utilizing forces of higher magnitude should be utilized to excite higher buckling modes in the structure. Although, in this study, the deformed profiles that were observed correspond to the first buckling mode, higher buckling modes may rejuvenate more resonant frequencies and therefore lead to an even more significant mitigation of the viscoelastic behavior. As modifying the dimensions of the unit cells may also provide similar effects, scaling analysis should also be investigated under the scope of different buckling modes.

4. Conclusions

In summary, in this study, we demonstrated the design of 3D structures encompassing intrinsic and external instabilities, leading to a remarkable enhanced dynamic behavior. The tested unit cells and their respective assemblies were investigated under the scope of a functional behavior that facilitates large deformations due to vibrations, instead of static loading or wave mechanics that are reported before. Prebuckling of the beam members of the structures provided augmented flexibility, mitigating the viscoelastic effects of the used rubber materials. Designing smart structures that furnish prebuckling before loading provides a new design parameter that can be tailored to improve the structural performance of such systems. Simulations and experiments on 3D-printed samples revealed that by connecting the unit cells next to each other, more resonant frequencies are rejuvenated. These results provide the guidelines to control the dynamic effects of 3D-printed elastomer materials. Nevertheless, it is evident that the design of these systems is highly complex. Optimization techniques[40–42] such as machine learning can be a useful arsenal to accomplish the objective to find the best design of the desired behavior. In addition, these effects may be incorporated even at smaller scales, for the design of microscale metamaterials. This study aims to provide the experimental and numerical approaches that have to be used for the modeling of the dynamic behavior of flexible structures. Finally, our findings pave the way to design smart materials, synergistically coupling rigidity and flexibility on demand, that are also expedient to the caducity of the working environment, such as mechanical signal transport or artificial muscles.

5. Experimental Section and Dynamic Modeling

A detailed description of the experimental procedure used to fabricate the samples and characterize their mechanical response, along with the dynamic modeling of these systems, can be found in the Supporting Information.

Supporting Information

Supporting Information is available from the Wiley Online Library or from the author.

Acknowledgements

All authors contributed equally in the experimental and theoretical results. All authors discussed the results and commented on the preparation of the manuscript. The authors thank Minok Park of the Laser Thermal Lab for assisting in the preparation of the imaging apparatus and Sedat Pala of the Liwei Lin Lab for his advice on the vibration generator that is needed. The authors thank Professor Fai Ma, Department of Mechanical Engineering, UC Berkeley, for his guidance regarding the experimental results. The authors also thank Nathaniel N. Goldberg and Evan Hemingway of the Dynamics Lab for providing critical arguments regarding the associated mechanical responses.

Conflict of Interest

The authors declare no conflict of interest.

Keywords

architected metamaterials, augmented resonance, prebuckling, tailored instabilities, 3D printing

Received: December 23, 2019
Revised: February 23, 2020
Published online: March 24, 2020

[1] A. A. Zadpoor, *Mater. Horizon* **2016**, *3*, 371.
[2] Y.-F. Zhang, N. Zhang, H. Hingorani, N. Ding, D. Wang, C. Yuan, B. Zhang, G. Gu, Q. Ge, *Adv. Funct. Mater.* **2019**, *29*, 1806698.
[3] Q. Chen, X. Zhang, B. Zhu, *Struct. Multidisc. Optim.* **2018**, *58*, 1395.
[4] Q. Chen, J. Zhao, J. Ren, L. Rong, P.-F. Cao, R. C. Advincula, *Adv. Funct. Mater.* **2019**, *29*, 1900469.
[5] D. Chen, X. Zheng, *Sci. Rep.* **2018**, *8*, 9139.
[6] A. S. Gladman, E. A. Matsumoto, R. G. Nuzzo, L. Mahadevan, J. A. Lewis, *Nat. Mater.* **2016**, *15*, 413.
[7] M. Lopez-Valdeolivas, D. Liu, D. J. Broer, C. Sanchez-Somolinos, *Macromol. Rapid Commun.* **2018**, *39*, 1700710.
[8] A. Rafsanjani, K. Bertoldi, A. R. Studart, *Sci. Robot.* **2019**, *4*, eaav7874.
[9] T. J. Wallin, J. Pikul, R. F. Shepherd, *Nat. Rev. Mater.* **2018**, *3*, 84.
[10] C. Christianson, N. N. Goldberg, D. D. Deheyn, S. Cai, M. T. Tolley, *Sci. Robot.* **2018**, *3*, eaat1893.
[11] Q. Ge, A. H. Sakhaei, H. Lee, C. K. Dunn, N. X. Fang, M. L. Dunn, *Sci. Rep.* **2016**, *6*, 31110.
[12] S. W. Pattinson, M. E. Huber, S. Kim, J. Lee, S. Grunsfeld, R. Roberts, G. Dreifus, C. Meier, L. Liu, N. Hogan, A. John Har, *Adv. Funct. Mater.* **2019**, *29*, 1901815.
[13] M. Kanik, S. Orguc, G. Varnavides, J. Kim, T. Benavides, D Gonzalez, T. Akintilo, C. C. Tasan, A. P. Chandrakasan, Y. Fink, P. Anikeeva, *Science* **2019**, *365*, 145.
[14] S. M. Mirvakili, I. W. Hunter, *Adv. Mater.* **2018**, *30*, 1704407.
[15] Y. Qiu, E. Zhang, R. Plamthottam, Q. Pei, *Acc. Chem. Res.* **2019**, *52*, 316.
[16] C. Coulais, D. Sounas, A. Alu, *Nature* **2017**, *542*, 461.
[17] N. Nadkarni, C. Daraio, D. M. Kochmann, *Phys. Rev. E* **2014**, *90*, 023204.
[18] R. Fleury, D. L. Sounas, C. F. Sieck, M. R. Haberman, A. Alu, *Science* **2014**, *343*, 516.
[19] S. Shan, S. H. Kang, J. R. Raney, P. Wang, L. Fang, F. Candido, J. A. Lewis, K. Bertoldi, *Adv. Mater.* **2015**, *27*, 4296.
[20] B. Deng, C. Mo, V. Tournat, K. Bertoldi, J. R. Raney, *Phys. Rev. Lett.* **2019**, *123*, 024101.

[21] C. Tawk, M. In Het Panhuis, G. M. Spinks, G. Alici, *Soft Robot.* **2018**, *5*, 685.
[22] Y. Mao, K. Yu, M. S. Isakov, J. Wu, M. L. Dunn, H. J. Qi, *Sci. Rep.* **2015**, *5*, 13616.
[23] W. Y. Yeong, N. Sudarmadji, H. Y. Yu, C. K. Chua, K. F. Leong, S. S. Venkatraman, Y. C. F. Boey, L. P. Tan, *Acta Biomater.* **2010**, *6*, 2028.
[24] B. N. Peele, T. J. Wallin, H. Zhao, R. F. Shepherd, *Bioinspir. Biomim.* **2015**, *10*, 055003.
[25] S. Kamrava, D. Mousanezhad, H. Ebrahimi, R. Ghosh, *Sci. Rep.* **2017**, *7*, 46046.
[26] A. Rafsanjani, A. Akbarzadeh, D. Pasini, *Adv. Mater.* **2015**, *27*, 5931.
[27] W. N. Findley, J. S. Lai, K. Onaran, *Creep and Relaxation of Nonlinear Viscoelastic Materials*, 1st ed., Dover Publications, Mineola, NY **1976**.
[28] T. Chen, O. R. Bilal, K. Shea, C. Daraio, *PNAS* **2018**, *113*, 5698.
[29] J. R. Raney, N. Nadkarni, C. Daraio, D. M. Kochmann, J. A. Lewis, K. Bertoldi, *Proc. Natl. Acad. Sci. USA* **2016**, *113*, 9722.
[30] M. H. Ghayesh, *Int. J. Eng. Sci.* **2018**, *124*, 115.
[31] A. Orlowska, C. Graczykowski, A. Galezia, *J. Compos. Mater.* **2017**, *52*, 2115.
[32] Z. Vangelatos, G. X. Gu, C. P. Grigoropoulos, *Extreme Mech. Lett.* **2019**, *33*, 100580.
[33] A. N. Norris, *Proc. R. Soc. A* **2014**, *470*, 20140522.
[34] Z. Vangelatos, V. Melissinaki, M. Farsari, K. Komvopoulos, C. Grigoropoulos, *Math. Mech. Solids* **2019**, *24*, 2636.
[35] K. K. Raju, G. V. Rao, *J. Struct. Eng.* **1986**, *112*, 433.
[36] S. G. Kelly, *Mechanical Vibrations: Theory and Applications*, Cengage Learning, Boston, MA **2012**.
[37] L. Meirovitch, *Analytical Methods in Vibrations*, 1st ed., Macmillan Publishing, New York, NY **1967**.
[38] I. M. Ward, J. Sweeney, *An Introduction to the Mechanical Properties of Solid Polymers*, 2nd ed., John Wiley & Sons, Hoboken, NJ **2004**.
[39] M. Brandenbourger, X. Locsin, E. Lerner, C. Coulais, *Nat. Commun.* **2019**, *10*, 4608.
[40] C. T. Chen, G. X. Gu, *MRS Commun.* **2019**, *9*, 556.
[41] L G. X. Gu, Z. Q. Dimas, M. J. Buehler, *J. Appl. Mech.* **2016**, *83*, 071006.
[42] G. X. Gu, M. J. Buehler, *Acta Mech.* **2018**, *229*, 4033.